CRYSTAL GROWTH & DESIGN

Article

pubs.acs.org/crystal

Spatial Control of Zeolitic Imidazolate Framework Growth on Flexible Substrates

Constantinos Dimitrakakis,[†,‡] Christopher D. Easton,[†] Benjamin W. Muir,[†] Bradley P. Ladewig,[‡] and Matthew R. Hill*[,†]

[†]Division of Materials Science and Engineering, CSIRO, Private Bag 10, Clayton South MDC, VIC 3169 Australia

[‡]Department of Chemical Engineering, Monash University, 1-131 Wellington Road, Clayton, VIC 3800 Australia

Supporting Information

ABSTRACT: The application of patterned thin film layers of metal organic frameworks onto surfaces is a matter of much interest of late with a view toward opening exciting applications for MOFs in gas sensing and catalysis. Here, the use of a plasma polymer coating technique has been employed to selectively alter the surface chemistry of a fibrous PTFE substrate to modify the in situ growth of ZIF-9 crystals over the surface, leading to the ability to control growth by promoting or inhibiting growth over desired regions on the polymer surface through the use of different coatings. XPS analysis of the surface elemental composition across regularly arranged regions of plasma polymer coverage has been extensively used to determine the mechanism of action. The immobilization of metallic cations on the surface by coordination with hydroxyl and carboxyl moieties in highly oxygenated diglyme-based plasma polymer coatings are proposed as favored nucleation points for solvothermal ZIF-9 growth. In contrast, amine-containing plasma polymer coatings based on allylamine serve to inhibit ZIF-9 growth through a lack of coordinating species on the surface, leaving the cobalt salt precursor unbound to the surface.

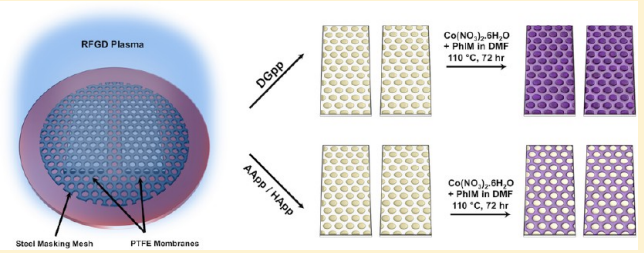

INTRODUCTION

Metal−organic frameworks (MOFs) are an emergent class of material with highly ordered one-, two-, or three-dimensional structures consisting of metal sites linked together by organic linker molecules, producing ultrahigh-porosity cage networks with pore dimensions of 0.5−5 nm and internal surface areas of several thousand square meters per gram.[1] These properties make them suitable for a wide variety of gas handling and processing applications, including storage,[2] continuous separation (for pre- or postcombustion carbon capture among many others),[3] or gas sensing and catalysis.[4] By simply changing the metal site or organic linker molecule, a vast number of different MOF structures are theoretically possible with a small fraction of these having been synthesized and characterized to date.[5] Within this sea of opportunity, a specific class centered around imidazolate-based linkers called zeolitic imidazolate frameworks (ZIFs) have emerged as a key focus of research due to their propensity to adopt structures analogous to known zeolite nets and their high chemical and thermal stability.[6] In contrast to zeolites, ZIFs contain pore windows on a smaller scale, on the order of 3−4 Å and similar to the kinetic diameters of many simple gas molecules, which allow them to behave as size-exclusive molecular sieves leading to great interest in their use for gas separation and storage.[7] The desired properties of a ZIF can be fine-tuned through careful selection of the coordinating metal[8] or the functional groups[9] on the ligand of a ZIF. Efforts in applying MOF and ZIF thin films onto surfaces are well-advanced,[10] typically onto hollow-fiber supports[11] or on inorganic flat sheet materials,[12] with a view to producing membranes suitable for industrial gas separation applications to replace existing energy-intensive systems. Thin film growth can be quickly achieved through seeded,[13] microwave-induced,[14] or contra-diffusion[15] growth, although advanced techniques are known that allow for extremely thin and defect-free films to be produced.[16]

The application of MOFs onto a surface in a controlled or patterned manner has been a topic of much interest of late. By controlling the positioning of MOFs on a surface, many additional applications beyond gas storage and separation become available where the MOF is responsive to external stimuli, such as the presence of gases,[4b,17] emits[18] or responds[19] to light, or incorporates heterogeneities for multifunctional materials.[20] Recently, a top-down approach was demonstrated[21] in which the MOF was deposited on a photoresist layer, which was selectively exposed and hardened. However, all other successful approaches to MOF patterning have been from bottom-up approaches,[22] which can involve external controls such as electrochemical synthesis,[23] microcontact printing[24] and magnetic manipulation,[20b] or growth promotion methods, such as nanoparticle seeding[20c] or chemical surface modification.[25] Many of these modification techniques have been applied to inorganic rigid substrates such as silica, alumina, or

Received: May 31, 2013
Revised: August 23, 2013
Published: August 29, 2013

 © 2013 American Chemical Society dx.doi.org/10.1021/cg400842q | Cryst. Growth Des. 2013, 13, 4411−4417

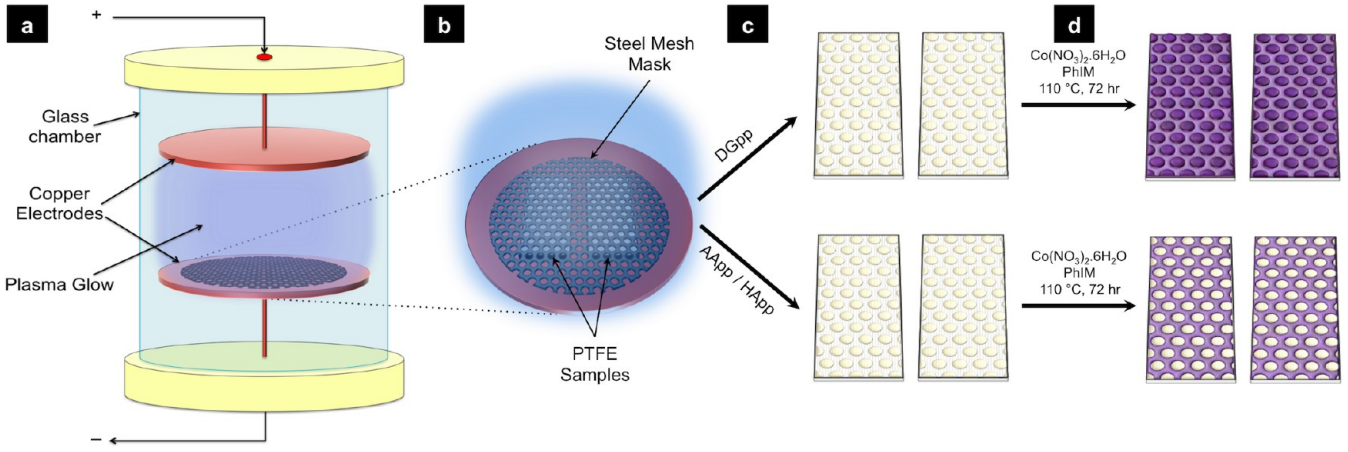

Figure 1. Schematic of RFGD plasma polymerization reactor and patterning process. (a) A voltage is applied between the copper electrodes, (b) ionizing the monomer vapor and generating a plasma glow discharge, (c) which results in a plasma polymer thin film coating on the PTFE samples. (d) After submersion in a ZIF-9 synthesis solution, the treated areas are either more (DGpp, top) or less (AApp/HApp, bottom) densely covered with ZIF-9 particles.

gold with the objective of promotion of the MOF growth in the desired areas but without much consideration of organic substrates such as polymer membranes or of exerting control to inhibit growth on regions where MOFs are not desired. This functionality would be useful in "lab-on-a-chip"-type applications where the MOF would need to be applied in an intricately patterned manner but with well-defined regions without MOF growth between the patterned areas. Such a process would enable these tailored surface chemical modifications to be utilized on a wider range of substrates. This would be a major step forward in MOF patterning technologies.

Radio frequency glow discharge (RFGD) plasma polymerization is a technique that is routinely employed to deposit thin polymer layers over numerous surfaces to influence their physical and chemical properties. This process generally involves[26] the application of an electrical potential difference across two copper electrodes (capacitively or inductively coupled) in the presence of an organic monomer vapor under low pressure. Application of a continuous radiofrequency voltage across the electrodes causes the monomer vapor to become a plasma which polymerizes and coats the sample. Traditionally, this technique has been utilized to control the interactions and binding of proteins to surfaces without requiring the protein itself to be present in the surface modification process[27] but has also been shown to be able to produce a platform for secondary functionalizations via click chemistry.[28] Patterning of the plasma polymer (PP) surface can be achieved directly in the deposition process using either a patterned top electrode[29] or a knife-edge electrode to create a PP gradient,[30] by employing a physical mask or photolithography[31] or in a post-treatment step using scanning probe nanolithography to etch a PP layer.[27] Many of the films of particular interest in protein patterning have utilized poly(ethylene oxide) (PEO), like PP films, to prevent nonspecific protein adsorption on the surface,[32] with the diethylene glycol dimethyl ether (also known as diglyme) monomer being one that has been exploited for this purpose.[33] Conversely, amine-containing PP films provide strong adsorbent sites for proteins.[34] Thus, precise control over regional surface chemistry is possible in either a positive or negative manner, as desired. Due to the adaptable and nondestructive nature of RFGD polymerization, it presents as a simple and quick process by which to alter the surface chemistry of a substrate beyond its traditional applications.

In this paper, we present a technique for the patterned growth of a ZIF-9 thin film on a porous polymeric substrate by selective modification of the surface chemistry using plasma polymerization. By this method, we have been able to produce intricate patterns on a surface that can either inhibit or promote the in situ growth of ZIF-9 ($Co(PhIM)_2 \cdot (DMF)(H_2O)$, PhIM = benzimidazolate, sodalite structure) (Figure 1). Using optimized PP film deposition conditions from previous studies, diglyme (DGpp), allylamine (AApp), and *n*-heptylamine (HApp)-based films were deposited on polytetrafluoroethylene (PTFE) substrates. We have found that the DGpp surface acts to promote ZIF growth via immobilization of cobalt ions on the surface. This does not occur on the AApp or HApp surfaces, which act to inhibit ZIF-9 growth instead.

EXPERIMENTAL SECTION

Materials and Synthesis. Allylamine (Sigma-Aldrich), *n*-heptylamine (Sigma-Aldrich), and diethylene glycol dimethyl ether (BDH) were used as monomers during RFGD deposition without further purification. Cobalt nitrate hexahydrate (Sigma-Aldrich), benzimidazole (Merck), and *N,N*-dimethylformamide (Merck) were used for ZIF-9 synthesis without further purification. The membranes used were commercially available polytetrafluoroethylene (PTFE) membrane sheets (on polypropylene backing) sourced from Membrane Solutions with a nominal pore size of 0.1 μm and a membrane thickness of 25−35 μm, cut into 5 × 2.5 cm rectangular samples and attached to glass slides using PTFE tape. The parameters chosen for RFGD plasma polymerization were a frequency of 200 kHz, load power of 20 W, initial monomer pressure of 20 Pa, and treatment time of 30 s. AApp and HApp coatings were performed in the same reactor chamber with a base vacuum pressure of 1 Pa; DGpp coatings were performed in a separate chamber with a base vacuum pressure of lower than 0.1 Pa. The PTFE samples were placed on the bottom electrode with masking provided by a stainless steel disc with a hexagonal array of ∼1.5 mm holes at ∼2.5 mm spacing. Growth of ZIF-9 on the modified PTFE surface was achieved using a synthesis procedure based on literature[7] by immersing the samples in a synthesis solution containing cobalt nitrate hexahydrate (0.2 g) and benzimidazole (0.6 g) in *N,N*-dimethylformamide (60 mL) (molar ratio $Co(NO_3)_2 \cdot 6H_2O$:PhIM:DMF = 1:7.39:1128) at 110 °C for 72 h. Subsequently, the samples were allowed to cool naturally to room temperature while still immersed and then removed from the synthesis mixture and

dx.doi.org/10.1021/cg400842q | *Cryst. Growth Des.* 2013, 13, 4411−4417

rinsed 3 times each with fresh DMF (20 mL) and methanol (20 mL) and left to dry in a vacuum oven overnight.

XRD Characterization. X-ray diffraction patterns were collected using a Rigaku Miniflex 600 X-ray diffractometer using Cu Kα radiation with a 0.01° step size at a rate of 1°/min on a separately prepared sample with a DGpp coating applied over the full surface of the PTFE membrane (i.e., without patterning) on a region with a dense coating of ZIF-9 crystals. An untreated PTFE sample was also analyzed as a reference.

XPS Characterization. Incubation of prepared PP surfaces for XPS characterisations were performed by dissolving either cobalt nitrate hexahydrate (0.33 g) or benzimidazole (1.0 g) in DMF (100 mL), incubating the sample in the solution at 110 °C for 1 h, rinsing 5 times with fresh DMF and drying in a vacuum oven for 1 h. X-ray photoelectron spectroscopy (XPS) analysis was performed using an AXIS Ultra DLD spectrometer (Kratos Analytical Inc., Manchester, U.K.) with a monochromated Al Kα source at a power of 180 W (15 kV × 12 mA), a hemispherical analyzer operating in the fixed analyzer transmission mode, and the standard aperture (analysis area: 0.3 × 0.7 mm). The total pressure in the main vacuum chamber during analysis was typically 10^{-8} mbar. Survey spectra were acquired at a pass energy of 160 eV. To obtain more detailed information about chemical structure, oxidation states, etc., high resolution spectra were recorded from individual peaks at 40 eV pass energy (yielding a typical peak width for polymers of 1.1−1.2 eV). Each specimen was analyzed at an emission angle of 0°, as measured from the surface normal. Assuming typical values for the electron attenuation length of relevant photoelectrons, the XPS analysis depth (from which 95% of the detected signal originates) ranges between 5 and 10 nm. Data processing was performed using CasaXPS processing software, version 2.3.15 (Casa Software Ltd., Teignmouth, U.K.). All elements present were identified from survey spectra. The atomic concentrations of the detected elements were calculated using integral peak intensities and the sensitivity factors supplied by the manufacturer. Binding energies were referenced to the aliphatic hydrocarbon peak at 285.0 eV. The accuracy associated with quantitative XPS is ca. 10−15%. Precision (i.e., reproducibility) depends on the signal/noise ratio but is usually much better than 5%. The latter is relevant when comparing similar samples. XPS images were acquired with a Mg Kα source at a power of 180 W (15 kV × 12 mA) at a pass energy of 160 eV in steps of 0.5 eV at a rate of 0.44 s/step using the field of view (FOV) 4 lens (~ 2.5 × 2.5 mm) in high-resolution mode. Long scans were performed under similar conditions at 25.26 s/step over reduced sweep ranges. For each image recorded, a corresponding background image was collected at approximately 20 eV away from the peak under investigation and subsequently used for background correction within Vision 2.0.

RESULTS AND DISCUSSION

ZIF-9 is of interest for its simple solvothermal synthesis technique, its high-modeled potential for H_2/CO_2 separation[3c] (similar to its zinc analogue ZIF-7), and its ability to "breathe" CO_2, exhibiting low uptake of the gas at low pressures but then opening up greatly at higher pressures,[35] while still taking up negligible amounts of N_2[36] or CH_4.[37] These interesting properties make it worthwhile for investigation for gas storage, separation, and sensing applications. PTFE mesh as a flexible substrate is suitably stable in the harsh ZIF-9 solvothermal growth conditions but attempts to nucleate and adhere ZIF-9 crystals to this inert material result in low surface coverage.

Remarkably, coverage of the PTFE surface with PP thin film coatings leads to preferred and nonpreferred areas of ZIF-9 growth (Figure 2), differing drastically in the coverage of ZIF-9 crystals on the surface after solvothermal growth. The ether-based DGpp delivers a surface that promotes growth of ZIF-9 compared to the native PTFE surface (Figure 2a), whereas the AApp- and HApp-patterned films lead to surfaces on which growth is inhibited relative to native PTFE (Figure 2b). Energy-

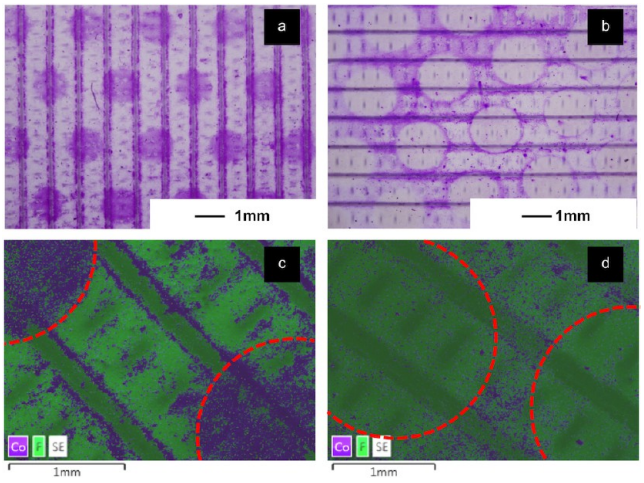

Figure 2. Imaging of PP-coated surfaces after ZIF-9 growth: DGpp-coated surface (a and c) and AApp-coated surface (b and d), under an optical microscope (a and b) and from EDX (c and d) showing cobalt in purple and fluorine in green and the circular PP-treated regions marked by a red dashed line.

dispersive X-ray spectroscopy (EDX) analysis of the positioning of cobalt (from ZIF-9) and fluorine (from PTFE) confirm the greater coverage and crystal growth of ZIF-9 on the DGpp-treated regions (Figure 2c) relative to the bulk PTFE. The reverse result is observed in the AApp and HApp systems with PP-coated regions showing low ZIF-9 growth (Figure 2d).

Scanning electron microscopy (SEM) images show this in greater detail (Figure 3), where the ZIF-9 coverage over the surfaces is compared between the bulk membrane surface away

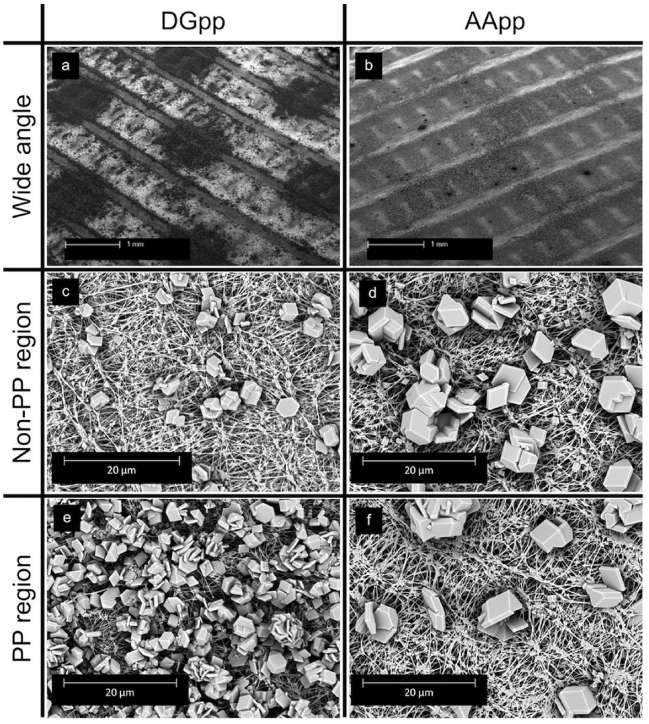

Figure 3. SEM imaging of PP-coated surfaces after ZIF-9 growth: DGpp-coated surfaces (left column) and AApp-coated surfaces (right column) from a wide, angled view (top row) and at the 4800× magnification away from and over the PP-treated regions (middle and bottom rows).

dx.doi.org/10.1021/cg400842q | Cryst. Growth Des. 2013, 13, 4411−4417

from PP-treated regions (Figure 3, panels c and d) and the treated circular areas (Figure 3, panels e and f). On the DGpp surface, it is apparent that the coating has greatly increased the number of nucleation points for ZIF-9 growth, resulting in numerous small crystals forming. On the AApp surface, the opposite is true, with nucleation greatly reduced, resulting in fewer, larger crystals forming. The coverage over the DGpp-treated area thus increased from 9.3% of the bulk untreated surface to approximately 54%, while on the AApp-treated surface the coverage dropped from 21.0% on the bulk untreated PTFE to 6.4% over the PP-coated areas. The discrepancy of the coverage over the untreated areas (9.3% away from DGpp vs 21% away from AApp) is a result of the different crystal sizes with a similar number of crystals present per unit area.

Thus, through the use of prefabricated masking disks to produce a pattern in the PP coverage over the surface, this method allows the controlled location of ZIF-9 particles on a surface, something that is crucial for the future application of these materials in devices or nanostructured membranes.[3c] This breakthrough leads to the controlled growth of ZIF crystals on surfaces simply through a facile, laboratory-based plasma pretreatment with a simple gaseous organic monomer precursor. A previous study has shown that edge resolution of approximately 10 μm is possible in a more ideal case involving physical masking of PP deposition on Si wafers.[31] However, the lower limit for resolution for masking on PTFE membranes is expected to be higher after taking into consideration the surface roughness of the membranes used and the profile of the masking plate.

This remarkable control was determined to be the result of the immobilization and activation of cobalt ions on the DGpp coating, leaving the metal ions amenable for coordination with the ZIF-9 benzimidazolate ligand. A series of experiments were undertaken to step through the patterned growth processes to be able to understand this mechanism. First, XPS imaging confirmed the fidelity of the nanometer-thick patterned PP surface on the PTFE substrate (Figure 4), with good edge definition (Figure 4, panels a and b), indicating that more intricate patterns could be obtainable. The DGpp coating introduces many ether linkages and exposed hydroxyl and acid moieties on the surface[30,38] (Figure 4c), while the AApp coating results in exposed amine functional groups (Figure 4d) with some oxygenated moieties expected to be present from trace amounts of oxygen gas in the low-pressure reactor chamber and oxidation of the film upon exposure to the atmosphere.

It is well-known that immobilized, activated metal ions on a surface will lead to promoted growth of MOF thin films.[22] To investigate this possibility, fresh samples of plasma-treated surfaces were exposed to solutions in DMF of the individual reactants, cobalt hydrate hexahydrate or benzimidazole, and analyzed via XPS survey scans across the PP-coated regions (Figure 5). After incubation of the PP-treated PTFE sheets in the Co-rich solution (Figure 5, panels a and b), the cobalt content increased in locations where the PP film was located (i.e., exposed holes). The higher relative suppression of the surface fluorine signal from the substrate below the AApp coating compared to the DGpp-coated surface indicates that the AApp coating constitutes a larger proportion of the probe volume of the measurement and is thus thicker than the DGpp film. A larger increase in the atomic percent (at. %) of cobalt on the patterned AApp coatings was observed when compared to

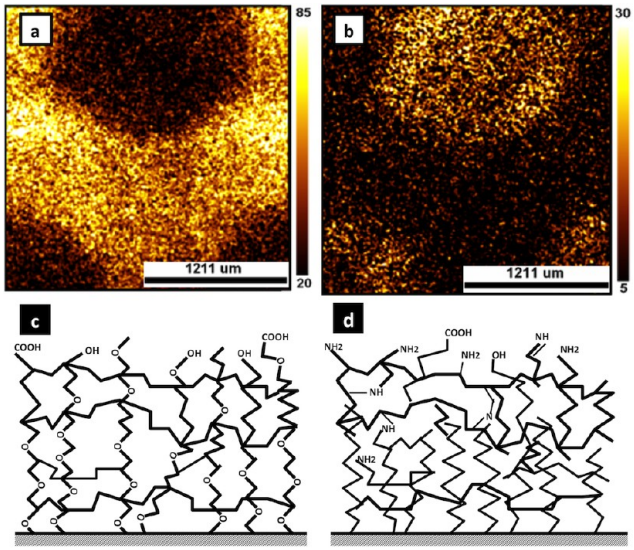

Figure 4. Characterization and illustration of the polymer coatings deposited on PTFE substrates by RFGD polymerization. XPS mapping of an AApp-treated PTFE surface confirms the successful deposition of the PP layer, showing regions of (a) suppressed fluorine surface content and (b) increased nitrogen content due to the presence of the film. (c) DGpp coating presents exposed hydroxyl and acid moieties, while the (d) AApp coating presents exposed amine moieties with oxygen-containing groups such as hydroxyls and acids.

the DGpp coating and is attributable to the increased thickness of the AApp film absorbing more of the cobalt nitrate salt.

Two peaks attributable to nitrogen were found during the scan of the AApp sample, at approximately 400 and 407 eV, and attributable to bound nitrogen atoms in amine groups and unbound nitrogen in nitrate ions, respectively. These were absent from the DGpp scan results (Figure 5c, blue trace, no intensity at ~407 eV), indicating that the PP coating is supplying charge neutrality and leaving the cobalt metal centers on the DGpp film in an altered coordination/complex state when compared to the AApp film. In a separate experiment, the detection limit for N was pushed to 0.01%, by reducing the sweep range while increasing the sweep time over the relevant binding energy range, confirming that no unbound nitrate ions were present for the DGpp sample (Figure 5d), with a small peak present at ~400 eV attributable to trace nitrogen contaminant bound to the surface.

In order for nitrate to be absent, another more strongly coordinating group must be present. PP coatings typically contain some oxygen species, even when oxygen is absent from the monomer employed, including hydroxyl and acid moieties due to postdeposition reactions with trapped radicals in the PP upon exposure to the atmosphere.[39] It is reasonable to expect that these oxygen species will be at a higher concentration in the DGpp coatings (which deliver preferred ZIF growth) when compared to the AApp coatings (which deliver nonpreferred ZIF growth). It was subsequently observed that the DGpp coatings contain an O/C ratio of 0.41, while the AApp contains an O/C ratio of 0.27 (excluding the contribution of carbon from the PTFE substrate but including the contribution of nitrate ions present). This finding can account for the absence of nitrate within the DGpp surface, as the immobilized cobalt ions are more favorably complexed by these additional oxygenated species by Coulombic interaction. The electron withdrawing nature of acid and hydroxyl moieties then facilitate

dx.doi.org/10.1021/cg400842q | Cryst. Growth Des. 2013, 13, 4411−4417

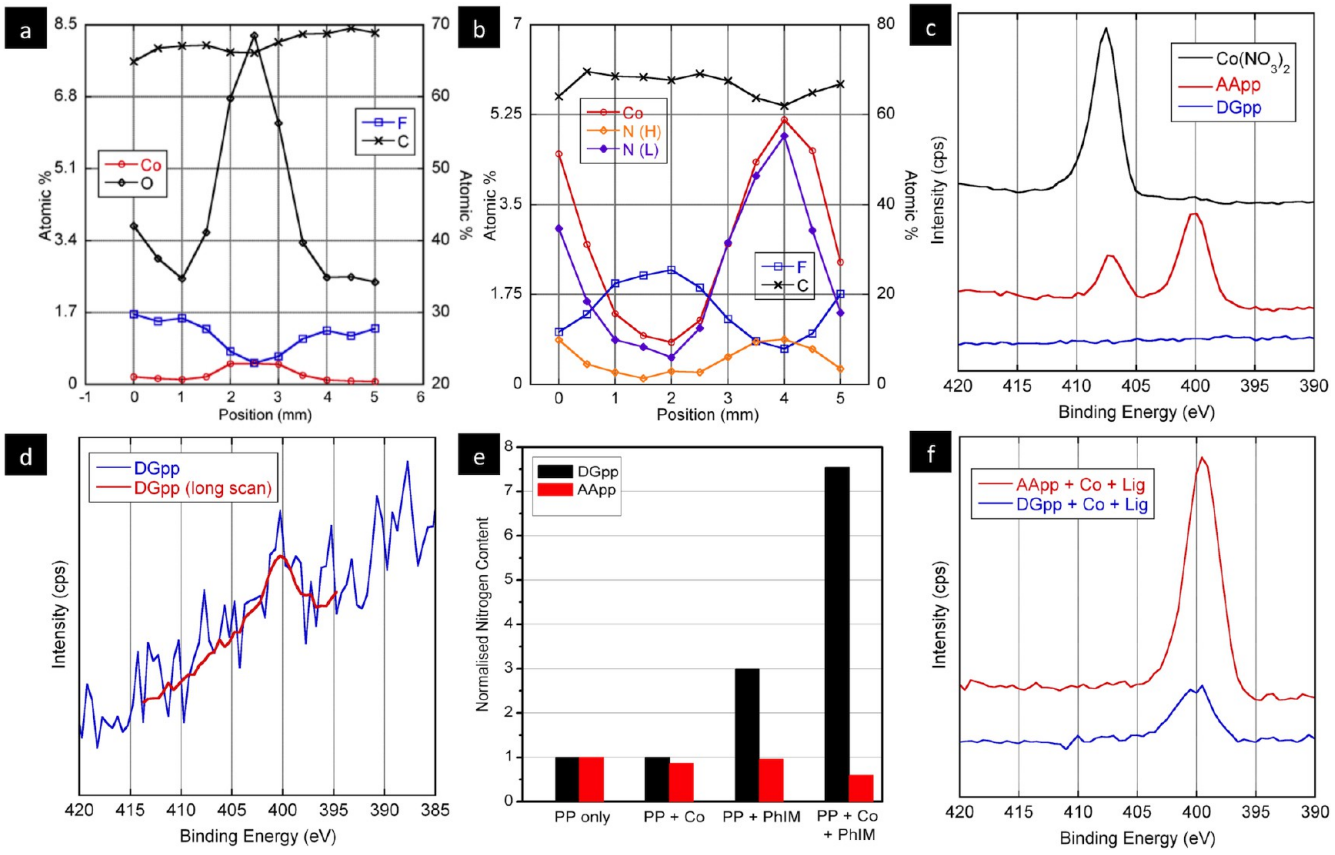

Figure 5. XPS analysis of ZIF surface layer film growth. Line scans across (a) a DGpp-patterned surface and (b) an AApp-patterned surface after incubating in cobalt nitrate solution show regular elemental surface concentration fluctuations. (c) Scans over the 390−420 eV range over the treated areas after the Co-incubation indicate the lack of bound nitrogen or unbound nitrates, with (d) longer scans (red line) showing only a small peak at 400 eV (equating to 0.15% N) attributable to the trace amine/amide contaminate. (e) The presence of immobilized cobalt on the DGpp surface from a Co incubation greatly increased the amount of nitrogen present after a subsequent incubation with PhIM compared to incubation with PhIM alone. The surface nitrogen content decreased after similar experiments on an AApp surface (results for DGpp and AApp are normalized against the nitrogen content in the respective untreated PPs, which are taken as 1). (f) After following a Co-incubation with a PhIM-incubation, the ∼407 eV peak is absent, indicating the rinsing of unbound nitrates present in (c) with only unbound PhIM present (∼ 400 eV).

the bound cobalt cations to be more reactive toward electron-rich species, such as the deprotonated ZIF-9 benzimidazolate ligand. This will result in a preferred growth of ZIF-9, by preconcentrating the reactants required for the thin film growth at the surface.

The situation on the AApp surface is somewhat different. Although cobalt ions are found on the AApp sample, which was found to inhibit growth of ZIF-9, the metal is present as the native nitrate salt, according to XPS analyses (Figure 5b). As a result, the cobalt ions would be labile and therefore able to leave the surface under solvothermal conditions. This would not promote MOF growth, and the metal species that remain on the surface would not be "activated" (as is the case in the DGpp films) to interact with the introduced benzimidazolate. To confirm that this was the case, a further control experiment was performed, exposing these cobalt-containing surfaces to benzimidazolate solutions under typical ZIF growth conditions, and assessing the change in nitrogen content following this treatment (Figure 5e). It was observed that the nitrogen content of Co- and PhIM-incubated DGpp samples increased 6-fold relative to the unincubated samples, whereas a slight decrease in nitrogen content was seen on the AApp surfaces after incubating with the Co- and PhIM-rich solutions relative to the PP-only sample. Further XPS analysis showed that the high-BE nitrogen peak at 407 eV on the Co-incubated AApp surface disappears after the subsequent PhIM incubation, as the unbound cobalt salts are rinsed away (Figure 5f). These factors lead to the preferred growth of ZIF-9 on patterned DGpp plasma polymer surfaces and nonpreferred growth on patterned AApp and HApp surfaces.

■ CONCLUSIONS

The application of a patterned layer of ZIF material on a polymer substrate by utilizing plasma polymers has been demonstrated to allow control of the growth of MOF particles on a surface. By utilizing XPS to map and analyze the surface elemental compositions of the samples at various stages of the ZIF-9 synthesis process, the immobilization and activation of metal ion MOF precursors was deduced to be the primary mechanism of action for the promotion of growth on the DGpp-coated PTFE surfaces. On the other hand, the AApp film was shown to be poor at forming complexes with the cobalt MOF precursor ions, leading to inhibited growth of ZIF-9 on such regions. The positional control afforded by this technique allows the user to selectively alter the MOF growth on specific surface regions to suit gas sensing, catalysis, and other "lab-on-a-chip"-style applications and marks a step forward in the growing field of MOF surface patterning technologies.

dx.doi.org/10.1021/cg400842q | Cryst. Growth Des. 2013, 13, 4411−4417

■ ASSOCIATED CONTENT

Supporting Information

Optical microscopy images, SEM images, and grazing incidence XRD patterns of ZIF-9 on PP-coated surfaces. This material is available free of charge via the Internet at http://pubs.acs.org.

■ AUTHOR INFORMATION

Corresponding Author

*E-mail: Matthew.Hill@csiro.au. Tel: +61 3 9545 2841.

Notes

The authors declare no competing financial interest.

■ ACKNOWLEDGMENTS

C.D. thanks the Australian Postgraduate Award Scheme for the provision of a scholarship.

■ ABBREVIATIONS

MOF, metal organic framework; ZIF, zeolitic imidazolate framework; RFGD, radio frequency glow discharge; PP, plasma polymer; DGpp, diglyme (diethylene glycol dimethyl ether)-based plasma polymer; AApp, allylamine-based plasma polymer; HApp, *n*-heptylamine-based plasma polymer; PTFE, polytetrafluoroethylene; SEM, scanning electron microscopy; EDX, energy-dispersive X-ray spectroscopy; XPS, X-ray photoelectron spectroscopy; DMF, *N*,*N*-dimethylformamide; PhIM, benzimidazole/benzimidazolate; BE, binding energy

■ REFERENCES

(1) Zhou, H.-C.; Long, J. R.; Yaghi, O. M. *Chem. Rev.* **2012**, *112* (2), 673−674.

(2) (a) Suh, M. P.; Park, H. J.; Prasad, T. K.; Lim, D.-W. *Chem. Rev.* **2012**, *112* (2), 782−835. (b) Sumida, K.; Hill, M. R.; Horike, S.; Dailly, A.; Long, J. R. *J. Am. Chem. Soc.* **2009**, *131* (42), 15120−15121.

(3) (a) Li, J.-R.; Sculley, J.; Zhou, H.-C. *Chem. Rev.* **2012**, *112* (2), 869−932. (b) Sumida, K.; Rogow, D. L.; Mason, J. A.; McDonald, T. M.; Bloch, E. D.; Herm, Z. R.; Bae, T.-H.; Long, J. R. *Chem. Rev.* **2012**, *112* (2), 724−781. (c) Thornton, A. W.; Dubbeldam, D.; Liu, M. S.; Ladewig, B. P.; Hill, A. J.; Hill, M. R. *Energy Environ. Sci.* **2012**, *5* (6), 7637−7646. (d) Nugent, P.; Belmabkhout, Y.; Burd, S. D.; Cairns, A. J.; Luebke, R.; Forrest, K.; Pham, T.; Ma, S.; Space, B.; Wojtas, L.; Eddaoudi, M.; Zaworotko, M. J. *Nature* **2013**, *495* (7439), 80−84.

(4) (a) Kreno, L. E.; Leong, K.; Farha, O. K.; Allendorf, M.; Van Duyne, R. P.; Hupp, J. T. *Chem. Rev.* **2012**, *112* (2), 1105−1125. (b) Lu, G.; Hupp, J. T. *J. Am. Chem. Soc.* **2010**, *132* (23), 7832−7833.

(5) Banerjee, R.; Phan, A.; Wang, B.; Knobler, C.; Furukawa, H.; O'Keeffe, M.; Yaghi, O. M. *Science* **2008**, *319* (5865), 939−943.

(6) Venna, S. R.; Carreon, M. A. *J. Am. Chem. Soc.* **2010**, *132* (1), 76−78.

(7) Park, K. S.; Ni, Z.; Côté, A. P.; Choi, J. Y.; Huang, R.; Uribe-Romo, F. J.; Chae, H. K.; O'Keeffe, M.; Yaghi, O. M. *Proc. Natl. Acad. Sci. U.S.A.* **2006**, *103* (27), 10186−10191.

(8) Biswal, B. P.; Panda, T.; Banerjee, R. *Chem. Commun.* **2012**, *48* (97), 11868−11870.

(9) Banerjee, R.; Furukawa, H.; Britt, D.; Knobler, C.; O'Keeffe, M.; Yaghi, O. M. *J. Am. Chem. Soc.* **2009**, *131* (11), 3875−3877.

(10) Bétard, A.; Fischer, R. A. *Chem. Rev.* **2012**, *112* (2), 1055−1083.

(11) Xu, G.; Yao, J.; Wang, K.; He, L.; Webley, P. A.; Chen, C.-s.; Wang, H. *J. Membr. Sci.* **2011**, *385*−*386* (0), 187−193.

(12) Li, Y.; Liang, F.; Bux, H.; Yang, W.; Caro, J. r. *J. Membr. Sci.* **2010**, *354* (1−2), 48−54.

(13) Li, Y.-S.; Liang, F.-Y.; Bux, H.; Feldhoff, A.; Yang, W.-S.; Caro, J. *Angew. Chem., Int. Ed.* **2010**, *49* (3), 548−551.

(14) Bux, H.; Liang, F.; Li, Y.; Cravillon, J.; Wiebcke, M.; Caro, J. r. *J. Am. Chem. Soc.* **2009**, *131* (44), 16000−16001.

(15) Yao, J.; Dong, D.; Li, D.; He, L.; Xu, G.; Wang, H. *Chem. Commun.* **2011**, *47* (9), 2559−2561.

(16) Motoyama, S.; Makiura, R.; Sakata, O.; Kitagawa, H. *J. Am. Chem. Soc.* **2011**, *133* (15), 5640−5643.

(17) (a) Achmann, S.; Hagen, G.; Kita, J.; Malkowsky, I.; Kiener, C.; Moos, R. *Sensors* **2009**, *9* (3), 1574−1589. (b) Chen, B.; Xiang, S.; Qian, G. *Acc. Chem. Res.* **2010**, *43* (8), 1115−1124.

(18) Cui, Y.; Yue, Y.; Qian, G.; Chen, B. *Chem. Rev.* **2012**, *112* (2), 1126−1162.

(19) (a) Modrow, A.; Zargarani, D.; Herges, R.; Stock, N. *Dalton Trans.* **2011**, *40* (16), 4217−4222. (b) Park, J.; Yuan, D.; Pham, K. T.; Li, J.-R.; Yakovenko, A.; Zhou, H.-C. *J. Am. Chem. Soc.* **2012**, *134* (1), 99−102. (c) Bernt, S.; Feyand, M.; Modrow, A.; Wack, J.; Senker, J.; Stock, N. *Eur. J. Inorg. Chem.* **2011**, *2011* (35), 5378−5383. (d) Lyndon, R.; Konstas, K.; Ladewig, B. P.; Southon, P. D.; Kepert, C. J.; Hill, M. R. *Angew. Chem., Int. Ed.* **2013**, *52* (13), 3695−8.

(20) (a) Buso, D.; Jasieniak, J.; Lay, M. D. H.; Schiavuta, P.; Scopece, P.; Laird, J.; Amenitsch, H.; Hill, A. J.; Falcaro, P. *Small* **2012**, *8* (1), 1−1. (b) Falcaro, P.; Normandin, F.; Takahashi, M.; Scopece, P.; Amenitsch, H.; Costacurta, S.; Doherty, C. M.; Laird, J. S.; Lay, M. D. H.; Lisi, F.; Hill, A. J.; Buso, D. *Adv. Mater.* **2011**, *23* (34), 3901−3906. (c) Falcaro, P.; Hill, A. J.; Nairn, K. M.; Jasieniak, J.; Mardel, J. I.; Bastow, T. J.; Mayo, S. C.; Gimona, M.; Gomez, D.; Whitfield, H. J.; Riccò, R.; Patelli, A.; Marmiroli, B.; Amenitsch, H.; Colson, T.; Villanova, L.; Buso, D. *Nat. Commun.* **2011**, *2*, 237. (d) Doherty, C. M.; Knystautas, E.; Buso, D.; Villanova, L.; Konstas, K.; Hill, A. J.; Takahashi, M.; Falcaro, P. *J. Mater. Chem.* **2012**, *22* (23), 11470−11474.

(21) Dimitrakakis, C.; Marmiroli, B.; Amenitsch, H.; Malfatti, L.; Innocenzi, P.; Grenci, G.; Vaccari, L.; Hill, A. J.; Ladewig, B. P.; Hill, M. R.; Falcaro, P. *Chem. Commun.* **2012**, *48* (60), 7483−7485.

(22) Falcaro, P.; Buso, D.; Hill, A. J.; Doherty, C. M. *Adv. Mater.* **2012**, *24* (24), 3153−3168.

(23) (a) Ameloot, R.; Pandey, L.; Auweraer, M. V. d.; Alaerts, L.; Sels, B. F.; De Vos, D. E. *Chem. Commun.* **2010**, *46* (21), 3735−3737. (b) Ameloot, R.; Stappers, L.; Fransaer, J.; Alaerts, L.; Sels, B. F.; De Vos, D. E. *Chem. Mater.* **2009**, *21* (13), 2580−2582.

(24) Ameloot, R.; Gobechiya, E.; Uji-i, H.; Martens, J. A.; Hofkens, J.; Alaerts, L.; Sels, B. F.; De Vos, D. E. *Adv. Mater.* **2010**, *22* (24), 2685−2688.

(25) (a) Yoo, Y.; Jeong, H.-K. *Chem. Commun.* **2008**, *21*, 2441−2443. (b) Zhuang, J.-L.; Ceglarek, D.; Pethuraj, S.; Terfort, A. *Adv. Funct. Mater.* **2011**, *21* (8), 1442−1447.

(26) Muir, B. W.; Nelson, A.; Fairbrother, A.; Fong, C.; Hartley, P. G.; James, M.; McLean, K. M. *Plasma Processes Polym.* **2007**, *4* (4), 433−444.

(27) Muir, B. W.; Fairbrother, A.; Gengenbach, T. R.; Rovere, F.; Abdo, M. A.; McLean, K. M.; Hartley, P. G. *Adv. Mater.* **2006**, *18* (23), 3079−3082.

(28) Chen, R. T.; Muir, B. W.; Such, G. K.; Postma, A.; Evans, R. A.; Pereira, S. M.; McLean, K. M.; Caruso, F. *Langmuir* **2010**, *26* (5), 3388−3393.

(29) Menzies, D. J.; Gengenbach, T.; Forsythe, J. S.; Birbilis, N.; Johnson, G.; Charles, C.; McFarland, G.; Williams, R. J.; Fong, C.; Leech, P.; McLean, K.; Muir, B. W. *Chem. Commun.* **2012**, *48* (13), 1907−1909.

(30) (a) Menzies, D. J.; Cowie, B.; Fong, C.; Forsythe, J. S.; Gengenbach, T. R.; McLean, K. M.; Puskar, L.; Textor, M.; Thomsen, L.; Tobin, M.; Muir, B. W. *Langmuir* **2010**, *26* (17), 13987−13994. (b) Menzies, D. J.; Jasieniak, M.; Griesser, H. J.; Forsythe, J. S.; Johnson, G.; McFarland, G. A.; Muir, B. W. *Surf. Sci.* **2012**, *606* (23,Äì24), 1798−1807.

(31) Mishra, G.; Easton, C. D.; McArthur, S. L. *Langmuir* **2010**, *26* (5), 3720−3730.

(32) Prime, K. L.; Whitesides, G. M. *J. Am. Chem. Soc.* **1993**, *115* (23), 10714−10721.

(33) Muir, B. W.; Tarasova, A.; Gengenbach, T. R.; Menzies, D. J.; Meagher, L.; Rovere, F.; Fairbrother, A.; McLean, K. M.; Hartley, P. G. *Langmuir* **2008**, *24* (8), 3828−3835.

(34) Kingshott, P.; McArthur, S.; Thissen, H.; Castner, D. G.; Griesser, H. J. *Biomaterials* **2002**, *23* (24), 4775−4785.
(35) Aguado, S.; Bergeret, G.; Titus, M. P.; Moizan, V.; Nieto-Draghi, C.; Bats, N.; Farrusseng, D. *New J. Chem.* **2011**, *35* (3), 546−550.
(36) Reyes, S. C.; Santiesteban, J. G.; Ni, Z.; Paur, C. S.; Kortunov, P.; Zengel, J.; Deckman, H. W. Separation of Carbon Dioxide from Nitrogen Utilizing Zeolitic Imidazolate Framework Materials. US 2009/0214407, 27/08.2009, 2009.
(37) Reyes, S. C.; Ni, Z.; Paur, C. S.; Kortunov, P.; Zengel, J.; Deckman, H. W.; Santiesteban, J. G. Separation of Carbon Dioxide from Methane Utilizing Zeolitic Imidazolate Framework Materials. US 2009/0211441, 27/08.2009, 2009.
(38) Menzies, D. J.; Nelson, A.; Shen, H.-H.; McLean, K. M.; Forsythe, J. S.; Gengenbach, T.; Fong, C.; Muir, B. W. *J. R. Soc. Interface* **2011**, *9*, 1008−1019.
(39) (a) Gengenbach, T. R.; Griesser, H. J. *Surf. Interface Anal.* **1998**, *26* (7), 498−511. (b) Gengenbach, T. R.; Griesser, H. J. *J. Polym. Sci., Part A: Polym. Chem.* **1998**, *36* (6), 985−1000.